Electronic Supplementary Information

Reactivity Difference in Oxidative Nucleophilic Reaction of Peroxonickel(III) Intermediates with Open-Chain and Macrocyclic Ligands

Seonggeun Yun,‡[a] Nam Kwon,‡[a] Seonghan Kim,[a] Donghyun Jeong,[a] Takehiro Ohta,[b,c] and Jaeheung Cho*[a]

[a]*Department of Emerging Materials Science, DGIST, Daegu 42988, Korea*

[b]*Picobiology Institute, Graduate School of Life Science, University of Hyogo, RSC-UHLP Center, Hyogo 679-5148, Japan*

[c]*Present Address: Department of Applied Chemistry, Faculty of Engineering, Sanyo-Onoda City University, Sanyo-Onoda, Yamaguchi 756-0884, Japan*

‡ *These authors contributed equally to this work.*

*Corresponding author: jaeheung@dgist.ac.kr

Experimental Section

Materials and Instrumentation. All chemicals obtained from Aldrich Chemical Co. were the best available purity and used without further purification unless otherwise indicated. The solvents acetonitrile (CH_3CN) and diethyl ether (Et_2O) were passed through solvent purification columns (JC Meyer Solvent Systems) prior to use. $H_2{}^{18}O_2$ (95% ^{18}O-enriched, 2.2% $H_2{}^{18}O_2$ in water) was purchased from ICON Services Inc. (Summit, NJ, USA).

UV-vis spectra were recorded on a Hewlett Packard 8453 diode array spectrophotometer equipped with a UNISOKU Scientific Instruments for low-temperature experiments or with a circulating water bath. Electrospray ionization mass spectra (ESI-MS) were collected on a Waters (Milford, MA, USA) Acquity SQD quadrupole Mass instrument, by infusing samples directly into the source using a manual method. The spray voltage was set at 2.5 kV and the capillary temperature at 80 °C. Resonance Raman spectra were obtained using a liquid nitrogen cooled CCD detector (CCD-1024×256-OPEN-1LS, HORIBA Jobin Yvon) attached to a 1-m single polychromator (MC-100DG, Ritsu Oyo Kogaku) with a 1200 groovs/mm holographic grating. An excitation wavelength of 441.6-nm was provided by a He-Cd laser (Kimmon Koha, IK5651R-G and KR1801C), with 20 mW power at the sample point. All measurements were carried out with a spinning cell at −60 °C. Crystallographic analysis was conducted with an SMART APEX II CCD equipped with a Mo X-ray tube at CCRF in DGIST. EPR spectra were also recorded at 77 K with the use of a JEOL X-band spectrometer (JES-FA200) at CCRF in DGIST. Product analysis was performed on a Thermo Fisher Trace 1310 gas chromatograph (GC) system equipped with a flame ionization detector (FID) and mass spectrometer (GC-MS).

Preparation of Complexes

[Ni(Me$_6$-trien)](ClO$_4$)$_2$. To an acetone solution (2 mL) of $Ni(ClO_4)_2{\cdot}6H_2O$ (0.37 g, 1 mmol), a acetone solution (2 mL) of Me$_6$-trien (0.23 g, 1 mmol) was added slowly. The mixture was stirred for overnight. The solvents were removed under vacuum to yield pink powder, which was recrystallized from acetone/Et_2O solution as a red product. Yield: 0.46 g (95%). UV-vis (acetone): λ_{max} (ε) = 500 nm (100 M^{-1} cm^{-1}). ESI-MS (acetone): *m/z* = 144.2 for $[Ni(Me_6\text{-trien})]^{2+}$. Anal. Calcd for $C_{12}H_{30}Cl_2N_4NiO_8$: C, 29.54; H, 6.20; N, 11.48. Found: C, 29.49; H, 6.53; N, 11.08. X-ray crystallographically suitable crystals were obtained by slow diffusion of Et_2O into acetone solution of $[Ni(Me_6\text{-trien})](ClO_4)_2$ in the presence of $NaBPh_4$.

[Ni(Me$_6$-trien)(NO$_3$)](BPh$_4$). To an acetone solution (2 mL) of $Ni(NO_3)_2{\cdot}6H_2O$ (0.29 g, 1 mmol), a acetone solution (2 mL) of Me$_6$-trien (0.23 g, 1 mmol) was added slowly. The mixture was stirred for overnight. The solvents were removed under vacuum to yield green powder, which was recrystallized from acetone/Et_2O solution as a green product. X-ray crystallographically suitable crystals were obtained by slow diffusion of Et_2O into acetone solution of the green product in the presence of $NaBPh_4$.

Crystalline yield: 0.44 g (65%). UV-vis (acetone): λ_{max} (ε) = 390 nm (46 M^{-1} cm^{-1}), 630 nm (24 M^{-1} cm^{-1}), 1040 nm (14 M^{-1} cm^{-1}). ESI-MS (acetone): *m/z* = 350.2 for $[Ni(Me_6\text{-trien})(NO_3)]^+$. Anal. Calcd for $C_{36}H_{50}BN_5NiO_3$: C, 64.50; H, 7.52; N, 10.45. Found: C, 64.30; H, 7.56; N, 10.45.

[Ni(12-TMC)(NO_3)](BPh_4)(H_2O). To an CH_3CN solution (2 mL) of $Ni(NO_3)_2{\cdot}6H_2O$ (0.29 g, 1 mmol), a CH_3CN solution (2 mL) of 12-TMC (0.23 g, 1 mmol) was added slowly. The mixture was refluxed for overnight. The solvents were removed under vacuum to yield blue powder, which was recrystallized from CH_3CN/Et_2O solution as a blue product. X-ray crystallographically suitable crystals were obtained by slow diffusion of Et_2O into CH_3CN solution of the blue product in the presence of $NaBPh_4$. Crystalline yield: 0.27 g (41%). UV-vis (acetone): λ_{max} (ε) = 375 nm (56 M^{-1} cm^{-1}), 590 nm (35M^{-1} cm^{-1}), 970 nm (34 M^{-1} cm^{-1}). ESI-MS (acetone): *m/z* = 348.2 for $[Ni(12\text{-TMC})(NO_3)]^+$. Anal. Calcd for $C_{36}H_{50}BN_5NiO_4$: C, 63.00; H, 7.34; N, 10.20. Found: C, 62.74; H, 6.90; N, 10.26.

Table S1. Crystal data and structure refinement for [Ni(Me$_6$-trien)](ClO$_4$)(BPh$_4$)((CH$_3$)$_2$CO), [Ni(Me$_6$-trien)(NO$_3$)](BPh$_4$) and [Ni(12-TMC)(NO$_3$)](BPh$_4$)

	[Ni(Me$_6$-trien)](ClO$_4$)(BPh$_4$)((CH$_3$)$_2$CO)	[Ni(Me$_6$-trien)(NO$_3$)](BPh$_4$)	[Ni(12-TMC)(NO$_3$)](BPh$_4$)
Empirical formula	$C_{39}H_{56}BClNiN_4O_5$	$C_{36}H_{50}BN_5NiO_3$	$C_{36}H_{48}BNiN_5O_3$
Formula weight	765.84	670.33	668.31
Temperature (K)	133(2)	133(2)	143(2)
Wavelength (Å)	0.71073	0.71073	0.71073
Crystal system/space group	orthorhombic, *Pna*2$_1$	Monoclinic, *P*2$_1$/*c*	orthorhombic, *Pna*2$_1$
Unit cell dimensions			
a (Å)	35.547(2)	11.6991(7)	29.560(3)
b (Å)	11.6830(7)	9.8702(6)	11.5592(14)
c (Å)	9.2810(6)	30.3175(16)	9.7924(11)
α (º)	90.00	90.00	90.00
β (º)	90.00	97.873(2)	90.00
γ (º)	90.00	90.00	90.00
Volume (Å^3)	3454.4(3)	3467.8(3)	3346.0(6)
Z	4	4	4
Calculated density (g/cm^{-3})	1.320	1.284	1.327
Absorption coefficient (mm^{-1})	0.620	0.602	0.624
Reflections collected	167965	161772	155805
Independent reflections [*R*(int)]	9597 [0.1506]	8706 [0.0822]	8401 [0.1668]
Refinement method	Full-matrix least-squares on F^2	Full-matrix least-squares on F^2	Full-matrix least-squares on F^2
Data/restraints/parameters	9597/1/469	8706/0/422	8401/1/419
Goodness-of-fit on F^2	1.146	1.094	0.973
Final *R* indices [*I* > 2sigma(*I*)]	R_1 = 0.0725 wR_2 = 0.1426	R_1 = 0.0644, wR_2 = 0.1457	R_1 = 0.0549, wR_2 = 0.1267
R indices (all data)	R_1 = 0.1039, wR_2 = 0.1546	R_1 = 0.0896, wR_2 = 0.1341	R_1 = 0.0881, wR_2 = 0.16432

Table S2. Selected bond distances (Å) and angles (º) for [Ni(Me_6-trien)](ClO_4)(BPh_4)((CH_3)$_2$CO), [Ni(Me_6-trien)(NO_3)](BPh_4) and [Ni(12-TMC)(NO_3)](BPh_4)

Bond Distances (Å)					
[Ni(Me_6-trien)](ClO_4)(BPh_4)((CH_3)$_2$CO)		[Ni(Me_6-trien)(NO_3)](BPh_4)		[Ni(12-TMC)(NO_3)](BPh_4)	
Ni-N1	1.944(5)	Ni-O1	2.151(2)	Ni-O1	2.141(4)
Ni-N2	1.925(4)	Ni-O2	2.117(2)	Ni-O2	2.143(4)
Ni-N3	1.928(5)	Ni-N1	2.158(3)	Ni-N1	2.134(3)
Ni-N4	2.003(6)	Ni-N2	2.078(3)	Ni-N2	2.084(4)
		Ni-N3	2.200(3)	Ni-N3	2.131(4)
		Ni-N4	2.148(3)	Ni-N4	2.085(5)
Bond Angles (°)					
[Ni(Me_6-trien)](ClO_4)(BPh_4)((CH_3)$_2$CO)		[Ni(Me_6-trien)(NO_3)](BPh_4)		[Ni(12-TMC)(NO_3)](BPh_4)	
N1-Ni-N2	86.80(2)	O1-Ni-O2	60.71(8)	O1-Ni-O2	60.23(13)
N1-Ni-N3	162.0(2)	N1-Ni-N2	85.19(10)	N1-Ni-N2	84.55(18)
N1-Ni-N4	102.9(3)	N1-Ni-N3	166.82(9)	N1-Ni-N3	160.34(14)
N2-Ni-N3	87.66(19)	N1-Ni-N4	88.08(13)	N1-Ni-N4	84.34(19)
N2-Ni-N4	161.4(3)	N2-Ni-N3	83.44(10)	N2-Ni-N3	83.88(18)
N3-Ni-N4	87.4(3)	N2-Ni-N4	109.23(11)	N2-Ni-N4	109.18(15)
		N3-Ni-N4	101.94(13)	N3-Ni-N4	84.53(19)
		Ni-O1-N5	91.36(16)	Ni-O1-N5	92.1 (3)
		Ni-O2-N5	92.37(17)	Ni-O2-N5	91.8 (3)

Table S3. Selected DFT parameters for $[Ni(Me_6\text{-trien})(O_2)]^+$ (**1**) and $[Ni(12\text{-TMC})(O_2)]^+$ (**2**)

Bond Distances (Å)			
1		**2**	
Ni-O1	1.88	Ni-O1	1.89
Ni-O2	1.93	Ni-O2	1.89
Ni-N1	2.22	Ni-N1	2.21
Ni-N2	2.10	Ni-N2	2.05
Ni-N3	2.25	Ni-N3	2.22
Ni-N4	2.09	Ni-N4	2.06
O1-O2	1.40	O1-O2	1.40
Bond Angles (°)			
1		**2**	
O1-Ni-O2	43.0	O1-Ni-O2	43.5
N1-Ni-N2	83.2	N1-Ni-N2	84.0
N1-Ni-N3	164.2	N1-Ni-N3	159.3
N1-Ni-N4	85.9	N1-Ni-N4	84.4
N2-Ni-N3	82.5	N2-Ni-N3	84.2
N2-Ni-N4	113.2	N2-Ni-N4	109.8
N3-Ni-N4	106.2	N3-Ni-N4	83.8

Table S4. Mulliken spin density on $Ni(O_{Total})^a$ of $[Ni(Me_6\text{-trien})(O_2)]^+$ (**1**) and $[Ni(12\text{-TMC})(O_2)]^+$ (**2**).

Model complex	1	2	3
1	36.0 (51.4)	64.5 (5.0)	47.9 (38.0)
2	36.1 (51.4)	65.8 (2.1)	46.2 (40.7)

[a]1, 2 and 3 represent the electron density composition of the *α-LUMO*, *β-LUMO* and *β-LUMO*+1 orbitals, respectively.

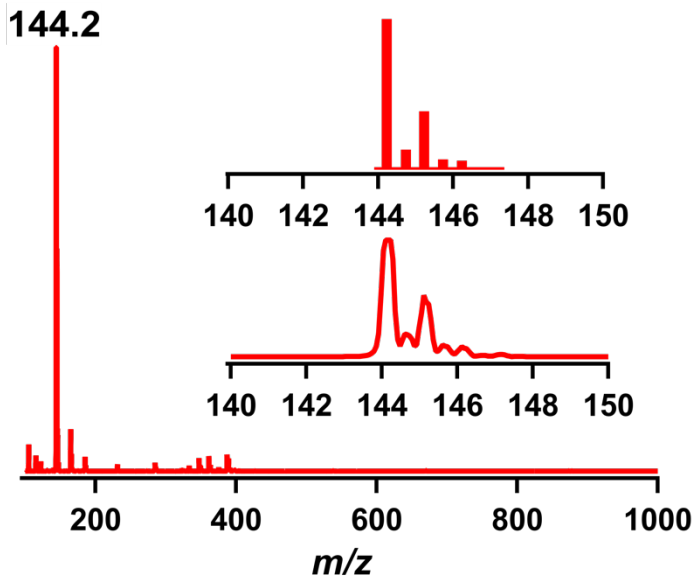

Fig. S1. ESI-MS spectrum of $[Ni(Me_6\text{-trien})](ClO_4)_2$ in acetone. Mass peak at *m/z* = 144.2 is assigned to $[Ni(Me_6\text{-trien})]^{2+}$ (calcd. *m/z* = 144.2). The inset shows the simulated (upper) and experimental (lower) isotope distribution patterns of the peak at *m/z* = 144.2.

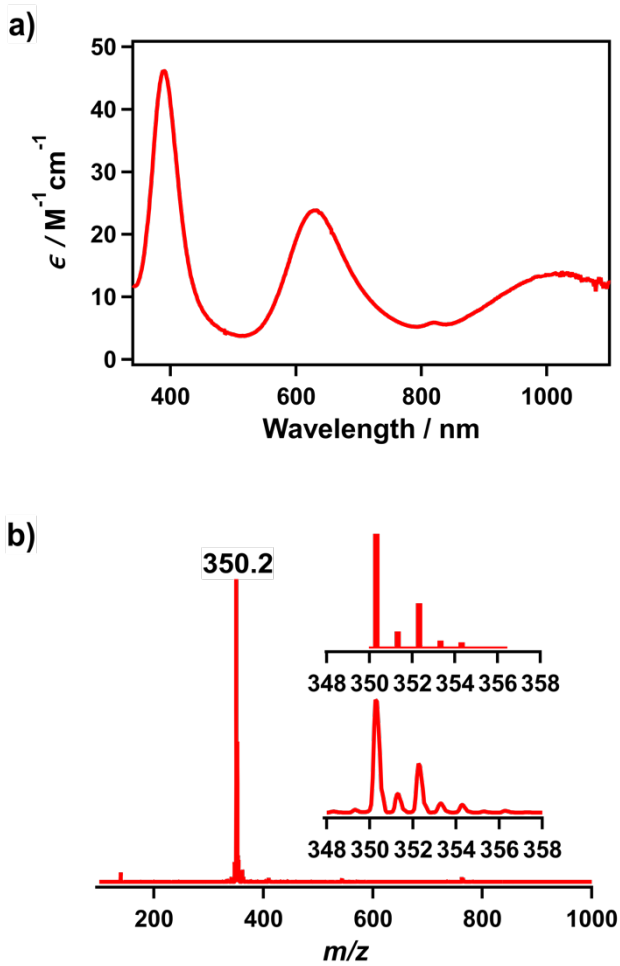

Fig. S2. (a) UV-vis spectrum of $[Ni(Me_6\text{-trien})(NO_3)]^+$ in acetone at –40 °C. (b) ESI-MS spectrum of $[Ni(Me_6\text{-trien})(NO_3)]^+$ in acetone. Mass peak at *m/z* = 350.2 is assigned to $[Ni(Me_6\text{-trien})(NO_3)]^+$ (calcd. *m/z* = 350.2). The inset shows the simulated (upper) and experimental (lower) isotope distribution patterns of the peak at *m/z* = 350.2.

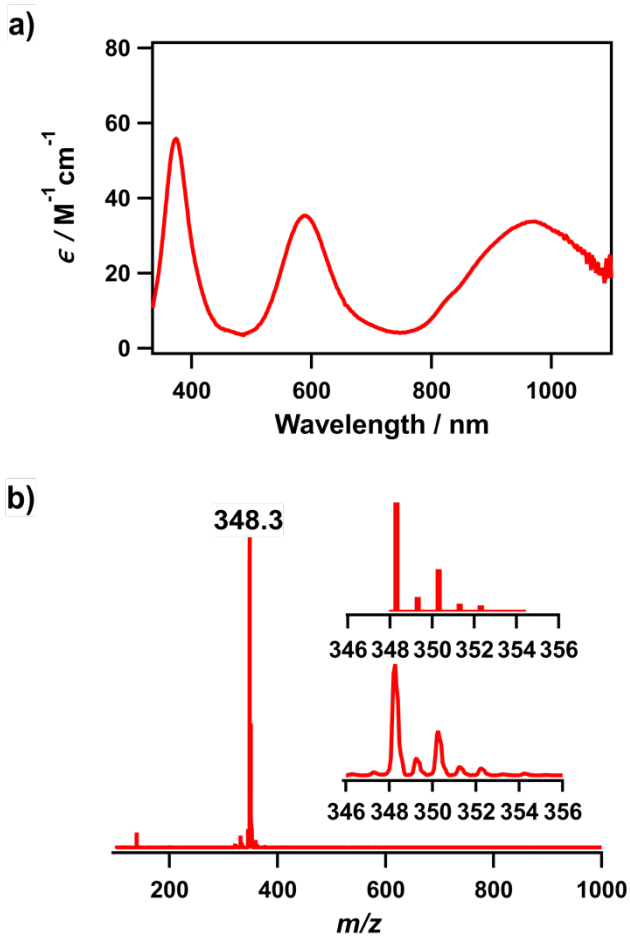

Fig. S3. (a) UV-vis spectrum of $[Ni(12\text{-}TMC)(NO_3)]^+$ in acetone at –40 °C. (b) ESI-MS spectrum of $[Ni(12\text{-}TMC)(NO_3)]^+$ in acetone. Mass peak at *m/z* = 348.3 is assigned to $[Ni(12\text{-}TMC)(NO_3)]^+$ (calcd. *m/z* = 348.3). The inset shows the simulated (upper) and experimental (lower) isotope distribution patterns of the peak at *m/z* = 348.3.

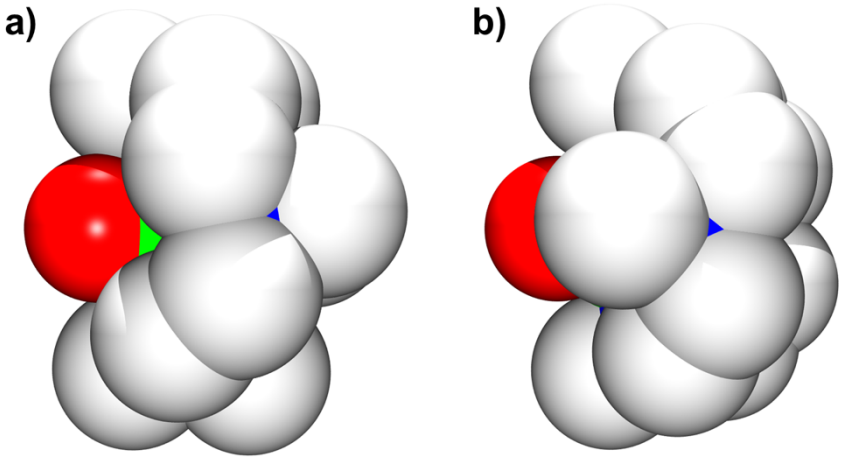

Fig. S4. Space-filling diagrams for the DFT-optimized structures of (a) $[Ni(Me_6\text{-trien})(O_2)]^+$ (**1**) and (b) $[Ni(12\text{-TMC})(O_2)]^+$ (**2**) (gray, C; blue, N; red, O; green, Ni). Hydrogen atoms are omitted for clarity.

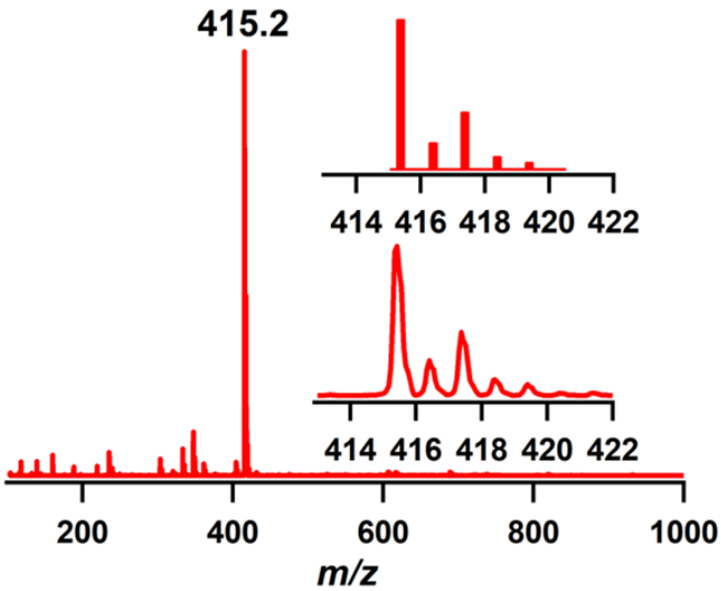

Fig. S5. ESI-MS spectrum taken after the completion of the reaction. Mass peak at *m/z* = 415.2 is assigned to $[Ni(Me_6\text{-trien})(HCOO)]^+$. The inset shows the simulated (upper) and experimental (lower) isotope distribution patterns of the peak at *m/z* = 415.2.

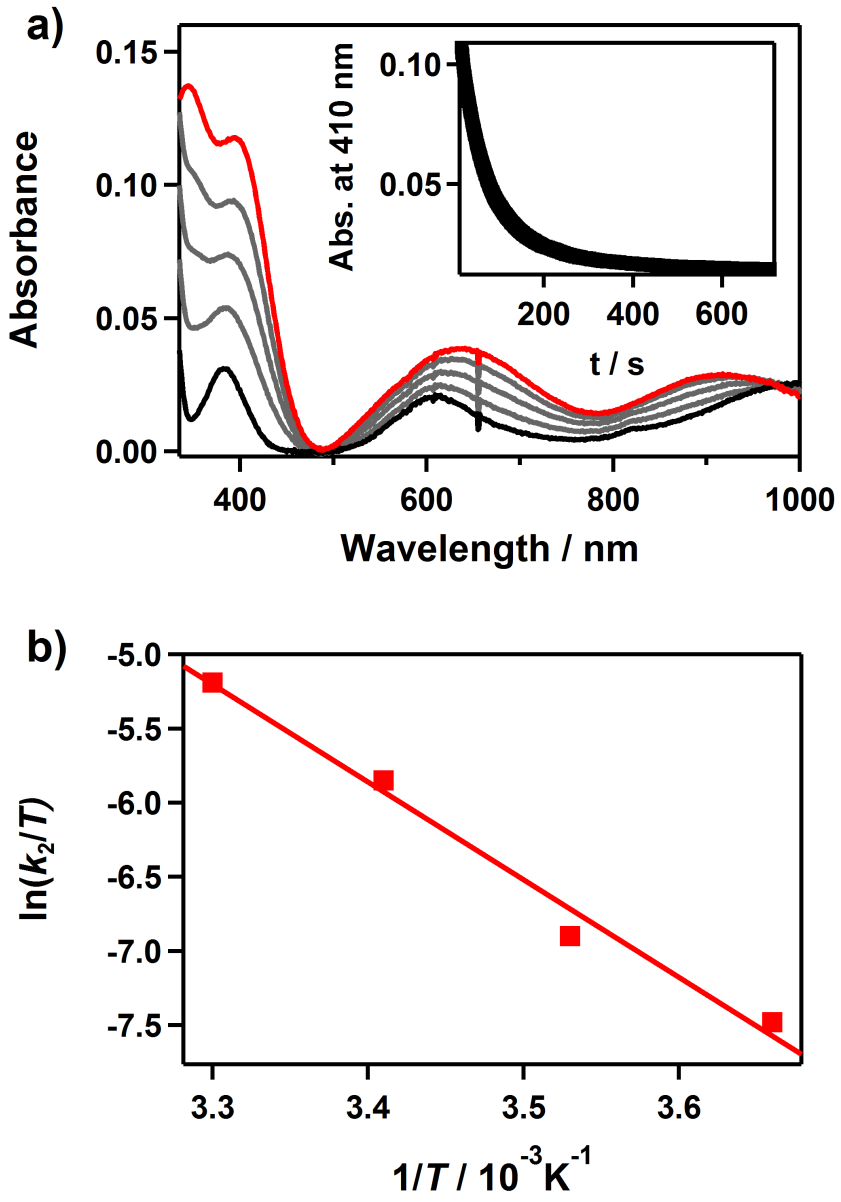

Fig. S6. Reactions of $[Ni(12\text{-}TMC)(O_2)]^+$ (**2**) with cyclohexylcarboxaldehyde (CCA). (a) UV-vis spectral changes of **2** (2 mM) upon addition of 40 equiv of CCA at 10 °C. Inset shows the time course of the absorbance at 410 nm (black). (b) Plot of first-order rate constants against $1/T$ to determine activation parameters.

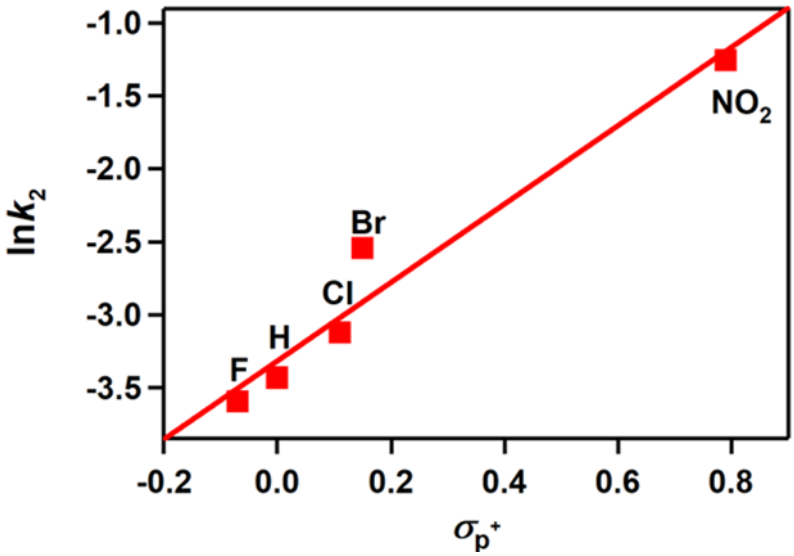

Fig. S7. Hammett plot of lnk_2 against σ_p^+ of benzoyl chloride derivatives in the reaction of [Ni(12-TMC)(O_2)]$^+$ (**2**) with *para*-substituted benzoyl chloride, *para*-X-Ph-COCl (X = F, H, Cl, Br, NO_2) in acetone at 10 ºC.

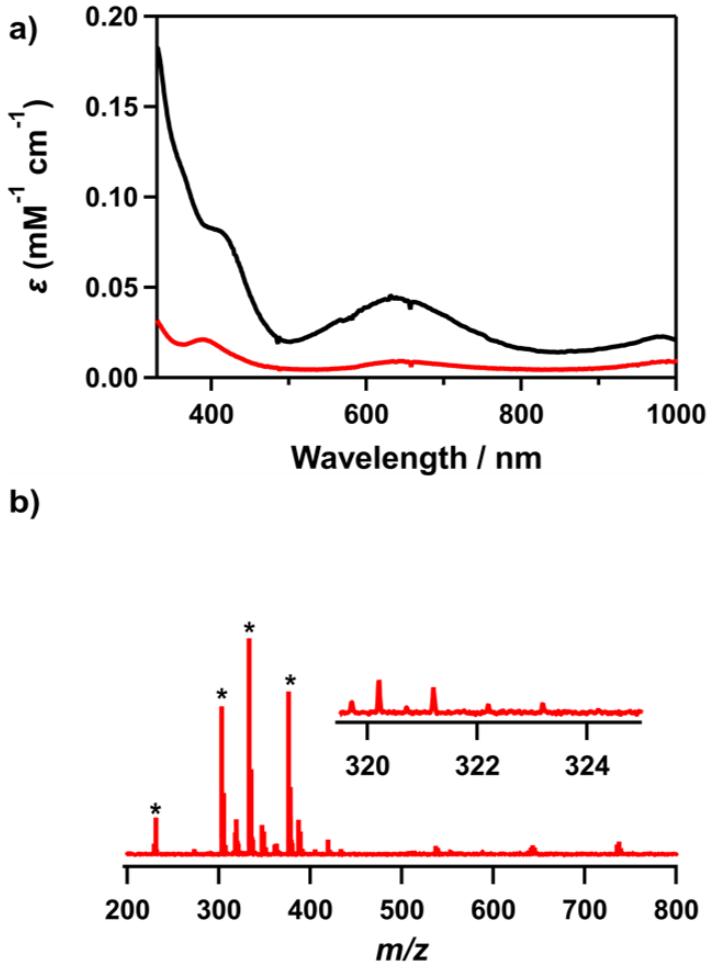

Fig. S8. (a) UV-vis spectra showing the formation of **1** in the reaction $[Ni(Me_6\text{-trien})(NO_3)]^+$ (2 mM; black line and 32 mM; red line) with 10 equiv of H_2O_2 and 5 equiv TEA in the presence of H_2O (9 M) in acetone at -50 °C. (b) CSI-MS spectrum of the reaction solution obtained in the reaction of $[Ni(Me_6\text{-trien})(NO_3)]^+$ with 10 equiv of H_2O_2 and 5 equiv TEA in the presence of H_2O (9 M) acetone at -50 °C. Asterisks are some unidentified species. The inset shows the expansion from 318 to 325 *m/z*.